Development of a Petascale Conservative Dynamical Core for Climate Simulation

Ram Nair

Computational Mathematics Group
Institute for Mathematics Applied to the Geosciences (IMAGe)
National Center for Atmospheric Research
Boulder CO 80305, USA.
(rnair@ucar.edu)

Turbulence and Dynamos at Petaspeed Symposium,
October 16th 2007, NCAR, Boulder

Overview

- Motivation
- Discontinuous Galerkin Methods (DGM)
  1. 1-D Case
  2. Extension to 2-D
- The DG Baroclinic Model (HOMME)
  1. Vertical aspects (Lagrangian Dynamics, Remapping)
  2. Horizontal Aspects (DGM, Discretization)
- Validation
  1. 2D Results
  2. 3D Results
- Parallel Performance
- Summary

Motivation

- Why do we need a new climate model?
- Because, the existing models have serious limitations to satisfy all of the following properties:
  1. Local and global conservation
  2. High-order accuracy
  3. High parallel efficiency
  4. Geometric flexibility ("Local" method)
  5. Monotonic (non-oscillatory) advection
- Discontinuous Galerkin Method (DGM) based model has the potential to address all of the above issues
- Recently, the Spectral Element (SE) model in HOMME shown to efficiently scale $\mathcal{O}$ (32, 000) processors on IBM BG/L.

Discontinuous Galerkin Method (DGM) in 1D

- 1D scalar conservation law:

$$\begin{aligned}\frac{\partial U}{\partial t} + \frac{\partial F(U)}{\partial x} &= 0 \quad \text{in} \quad \Omega \times (0, T), \\ U_0(x) &= U(x, t = 0), \quad \forall x \in \Omega\end{aligned}$$

- The domain Ω (periodic) is partitioned into N_x non-overlapping elements (intervals) $I_j = [x_{j-1/2}, x_{j+1/2}]$, $j = 1, \ldots, N_x$, and $\Delta x_j = (x_{j+1/2} - x_{j-1/2})$

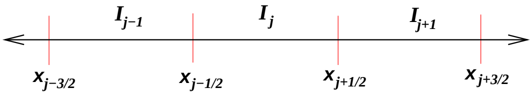

DGM-1D: Weak Formulation

A weak formulation of the problem for the approximate solution U_h is obtained by multiplying the PDE by a *test* function $\varphi_h(x)$ and integrating over an element I_j:

$$\int_{I_j} \left[\frac{\partial U_h}{\partial t} + \frac{\partial F(U_h)}{\partial x} \right] \varphi_h(x) dx = 0, \quad U_h, \varphi_h \in \mathcal{V}_h$$

Integrating the second term by parts $\implies$

$$\int_{I_j} \frac{\partial U_h(x,t)}{\partial t} \varphi_h(x) dx - \int_{I_j} F(U_h(x,t)) \frac{\partial \varphi_h}{\partial x} dx +$$
$$F(U_h(x_{j+1/2},t))\, \varphi_h(x^-_{j+1/2}) - F(U_h(x_{j-1/2},t))\, \varphi_h(x^+_{j-1/2}) = 0,$$

where $\varphi(x^-)$ and $\varphi(x^+)$ denote "left" and "right" limits

DGM-1D: Flux term (“Gluing” the discontinuous element edges)

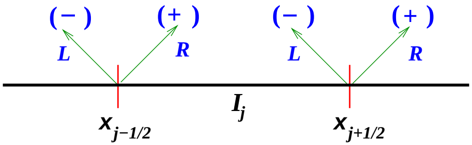

- Flux function $F(U_h)$ is discontinuous at the interfaces $x_{j\pm 1/2}$
- $F(U_h)$ is replaced by a numerical flux function $\hat{F}(U_h)$, dependent on the left and right limits of the discontinuous function U. At the interface $x_{j+1/2}$,

$$\hat{F}(U_h)_{j+1/2}(t) = \hat{F}(U_h(x^-_{j+1/2}, t), U_h(x^+_{j+1/2}, t))$$

- Typical flux formulae (Approx. Reimann Solvers): Gudunov, Lax-Friedrichs, Roe, HLLC, etc.

DGM-1D: Space Discretization

- Choose an orthogonal basis set $\mathcal{B}$ spanning the space V_h^k, s.t., approx. solution U_h and φ_h are in V_h^k.
- Use a high-order Gaussian quadrature such as the Gauss-Lobatto-Legendre (GLL) quadrature rule
- Map every element I_j onto the reference element $[-1, +1]$ by introducing a local coordinate $\xi \in [-1, +1]$ s.t.,

$$\xi = \frac{2\,(x - x_j)}{\Delta x_j},\; x_j = (x_{j-1/2} + x_{j+1/2})/2 \;\Rightarrow\; \quad \frac{\partial}{\partial x} = \frac{2}{\Delta x_j}\,\frac{\partial}{\partial \xi}.$$

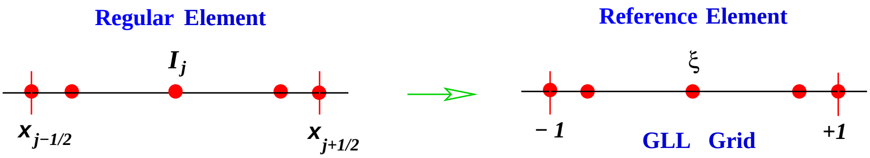

DGM-1D: Orthogonal Basis Set (Modal Vs Nodal)

- The model basis set consists of Legendre polynomials, $\mathcal{B} = \{P_\ell(\xi), \ell = 0, 1, \ldots, k\}$

$$
\begin{aligned}
U_j(\xi, t) &= \sum_{\ell=0}^{k} U_j^\ell(t)\, P_\ell(\xi) \quad \text{for} \quad -1 \le \xi \le 1, \quad \text{where} \\
U_j^\ell(t) &= \frac{2\ell+1}{2} \int_{-1}^{1} U_j(\xi, t)\, P_\ell(\xi)\, d\xi \quad \ell = 0, 1, \ldots, k.
\end{aligned}
$$

- The nodal basis set $\mathcal{B}$ is constructed using Lagrange-Legendre polynomials $h_i(\xi)$ with roots at Gauss-Lobatto quadrature points.

$$
\begin{aligned}
U_j(\xi) &= \sum_{j=0}^{k} U_j\, h_j(\xi) \quad \text{for} \quad -1 \le \xi \le 1, \\
h_j(\xi) &= \frac{(\xi^2 - 1)\, P_k'(\xi)}{k(k+1)\, P_k(\xi_j)\, (\xi - \xi_j)}.
\end{aligned}
$$

- In any case, the mass matrix is diagonal

DGM: Basis Functions

Spatial Discretization

- Gaussian Quadrature: $\int_{-1}^{1} \omega(x)p(x)dx = \sum_{i=0}^{n} w_i p(x_i)$
  GLL: $\omega(x) \equiv 1,\ x_0 = -1,\ x_n = 1$
- Interpolation: two options for basis functions

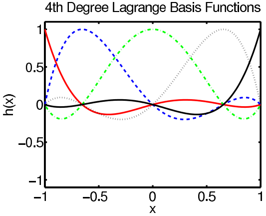

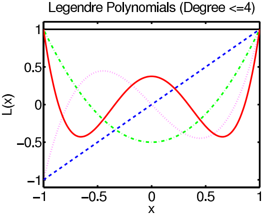

Nodal expansion: Lagrange basis

Modal expansion: Legendre basis

DGM: Explicit Time Integration

- Final Semi-discretized form $\Longrightarrow$

$$\frac{d}{dt}U_j = \mathcal{L}(U_j) \quad \text{in} \quad (0, T)$$

- Strong Stability Preserving third-order Runge-Kutta (SSP-RK) scheme (*Gottlieb et al., 2001*)

$$\begin{aligned} U^{(1)} &= U^n + \Delta t \mathcal{L}(U^n) \\ U^{(2)} &= \frac{3}{4}U^n + \frac{1}{4}U^{(1)} + \frac{1}{4}\Delta t \mathcal{L}(U^{(1)}) \\ U^{n+1} &= \frac{1}{3}U^n + \frac{2}{3}U^{(2)} + \frac{2}{3}\Delta t \mathcal{L}(U^{(2)}). \end{aligned}$$

  where the superscripts n and $n+1$ denote time levels t and $t+\Delta t$, respectively

- Note: The Courant number for the DG scheme is estimated to be $1/(2k+1)$, where k is the degree of the polynomial, however, no theoretical proof exists when $k > 1$ (*Cockburn and Shu, 1989*).

DG-2D Spatial Discretization for an Element Ω

2D Scalar conservation law

$$\frac{\partial U}{\partial t} + \nabla \cdot \mathbf{F}(U) = S(U), \quad \text{in} \quad \Omega \times (0, T); \, \forall \, (x^1, x^2) \in \Omega$$

where $U = U(x^1, x^2, t)$, $\nabla \equiv (\partial/\partial x^1, \partial/\partial x^2)$, $\mathbf{F} = (F, G)$ is the flux function, and S is the source term.

- Weak Galerkin formulation: Multiplication of the basic equation by a *test function* $\varphi_h \in \mathcal{V}_h$ and integration over an element Ω.

$$\frac{\partial}{\partial t} \int_\Omega U_h \, \varphi_h \, d\Omega - \int_\Omega \mathbf{F}(U_h) \cdot \nabla \varphi_h \, d\Omega \quad + \int_\Gamma \mathbf{F}(U_h) \cdot \vec{n} \, \varphi_h \, d\Gamma = \int_\Omega S(U_h) \, \varphi_h d\Omega$$

where U_h is an approximate solution in $\mathcal{V}_h$.

- Can be extended to a system of equations

DG-2D: The Flux Term

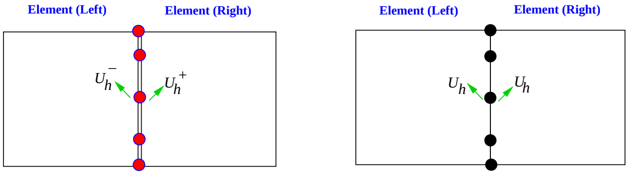

After Num. Flux Operation

- Along the boundaries (Γ) of an element the solution U_h is discontinuous (U_h^- and U_h^+ are the left and right limits).
- Therefore, the analytic flux $\mathbf{F}(U_h) \cdot \vec{n}$ must be replaced by a numerical flux such as the Lax-Friedrichs Flux:

$$\mathbf{F}(U_h) \cdot \vec{n} = \frac{1}{2}\left[(\mathbf{F}(U_h^-) + \mathbf{F}(U_h^+)) \cdot \vec{n} - \alpha(U_h^+ - U_h^-) \right].$$

- For the SW system, α is the upper bound on the absolute value of eigenvalues of the flux Jacobian $\mathbf{F}'(U)$; (*Nair et al., 2005*)
  $\alpha^1 = \max\left(|u^1| + \sqrt{\Phi\, G^{11}}\right), \quad \alpha^2 = \max\left(|u^2| + \sqrt{\Phi\, G^{22}}\right)$

The DG, SE & FV Methods

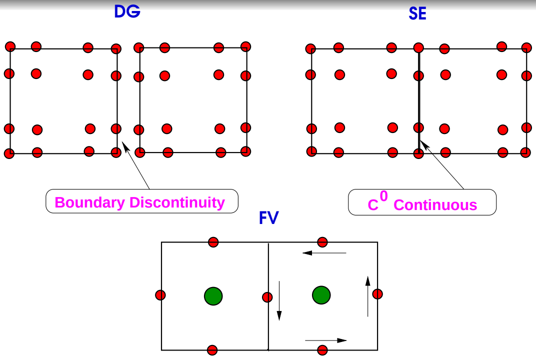

DGM is a hybrid approach (DG $\Leftarrow$ SE + FV)

- The domain $\mathcal{D}$ is partitioned into non-overlapping elements Ω_{ij} such that the element boundaries are discontinuous.
- Based on conservation laws but exploits the spectral expansion of SE method and treats the element boundaries using FV "tricks."

DG-2D: Spatial Discretization

High-order nodal basis set

- The nodal basis set is constructed using a tensor-product of Lagrange-Legendre polynomials ($h_i(\xi)$) with roots at Gauss-Lobatto quadrature points.

$$h_i(\xi) = \frac{(\xi^2 - 1)\, P'_N(\xi)}{N(N+1)\, P_N(\xi_i)\, (\xi - \xi_i)}; \qquad \int_{-1}^{1} h_i(\xi) h_j(\xi) = w_i \delta_{ij}.$$

where $P_N(\xi)$ is the N^{th} order Legendre polynomial, and w_i weights associated with the Gauss quadrature.

- The approximate solution (U_h) and test function (φ_h) are represented in terms of nodal basis set.

$$U_{ij}(\xi, \eta) = \sum_{i=0}^{N} \sum_{j=0}^{N} U_{ij}\, h_i(\xi)\, h_j(\eta) \quad \text{for} \quad -1 \leq \xi, \eta \leq 1,$$

- The nodal version was shown to be more computationally efficient than the modal in (*Dennis et al., 2006*).

DG-3D Model: Explicit Time Integration

- Final form for the nodal discretization leads to the ODE:

$$\frac{d}{dt}U_{ij}(t) = \frac{4}{\Delta x_i^1 \Delta x_j^2 \, w_i w_j} \left[I_{Grad} + I_{Flux} + I_{Source} \right],$$

- For a system of conservation laws, solve the ODE system:

$$\frac{d}{dt}\mathbf{U} = L(\mathbf{U}) \quad \text{in} \quad (0, T) \times \Omega$$

- Time integration: Explicit third-order Runge-Kutta (SSP) scheme (*Gottlieb et al., 2001*)
- Options for explicit diffusion (∇^2 or ∇^4).
- Boyd-Vandeevan spatial Filter
- Optional Monotonic Limiter (for scalar fields)

Scaling Plots

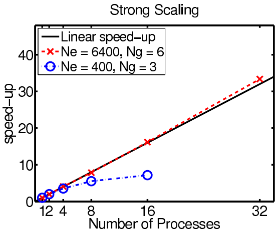

Strong scaling is measured by increasing the number of processes running while keeping the problem size constant.

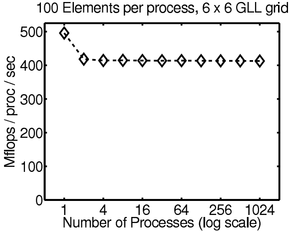

Weak scaling is measured by scaling the problem along with the number of processes, so that work per process is constant.

HOMME (High-Order Method Modeling Environment)

- The Discontinuous Galerkin (DG) model is the conservative option in the HOMME framework
- HOMME Grid: The sphere is decomposed into 6 identical regions, using the equiangular projection (*Sadourny, 1972*)
  - Local coordinate systems are free of singularities
  - Creates a non-orthogonal curvilinear coordinate system

Cubed Sphere Geometry: Logical cube-face orientation

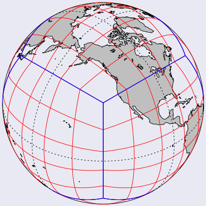

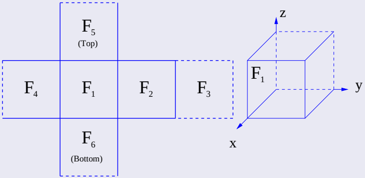

HOMME Grid System

Metric Tensor G_{ij}, [Cubed-Sphere $\rightleftharpoons$ Sphere] Transform

Central angles $x^1, x^2 \in [-\pi/4, \pi/4]$ are the independent variables.

$$G_{ij} = \frac{R^2}{\rho^4 \cos^2 x^1 \cos^2 x^2} \begin{bmatrix} 1 + \tan^2 x^1 & -\tan x^1 \tan x^2 \\ -\tan x^1 \tan x^2 & 1 + \tan^2 x^2 \end{bmatrix}$$

where $\rho^2 = 1 + \tan^2 x^1 + \tan^2 x^2$, $i, j \in \{1, 2\}$

- Metric tensor in terms of longitude-latitude (λ, θ):

$$G_{ij} = A^T A; \quad A = \begin{bmatrix} R\cos\theta\, \partial\lambda/\partial x^1 & R\cos\theta\, \partial\lambda/\partial x^2 \\ R\,\partial\theta/\partial x^1 & R\,\partial\theta/\partial x^2 \end{bmatrix}$$

- The matrix A is used for transforming spherical velocity (u, v) to the covariant (u_1, u_2) and contravariant (u^1, u^2) vectors.

Hydrostatic Prognostic Equations in Flux Form (Curvilinear coordinates)

$$\frac{\partial u_1}{\partial t} + \nabla_c \cdot \mathbf{E}_1 + \dot{\eta}\frac{\partial u_1}{\partial \eta} = \sqrt{G}u^2\,(f+\zeta) - R\,T\frac{\partial}{\partial x^1}(\ln p)$$

$$\frac{\partial u_2}{\partial t} + \nabla_c \cdot \mathbf{E}_2 + \dot{\eta}\frac{\partial u_2}{\partial \eta} = -\sqrt{G}u^1\,(f+\zeta) - R\,T\frac{\partial}{\partial x^2}(\ln p)$$

$$\frac{\partial}{\partial t}(m) + \nabla_c \cdot \left(\mathbf{U}^i\, m\right) + \frac{\partial(m\dot{\eta})}{\partial \eta} = 0$$

$$\frac{\partial}{\partial t}(m\Theta) + \nabla_c \cdot \left(\mathbf{U}^i\,\Theta\, m\right) + \frac{\partial(m\dot{\eta}\,\Theta)}{\partial \eta} = 0$$

$$\frac{\partial}{\partial t}(mq) + \nabla_c \cdot \left(\mathbf{U}^i\, q\, m\right) + \frac{\partial(m\dot{\eta}\, q)}{\partial \eta} = 0$$

$$m \equiv \sqrt{G}\,\frac{\partial p}{\partial \eta}, \nabla_c \equiv \left(\frac{\partial}{\partial x^1}, \frac{\partial}{\partial x^2}\right), \eta = \eta(p, p_s), G = \det(G_{ij}), \ \frac{\partial \Phi}{\partial \eta} = -\frac{R\,T}{p}\,\frac{\partial p}{\partial \eta}.$$

Where m is the mass function, Θ is the potential temperature and q is the moisture variable. $\mathbf{U}^i = (u^1, u^2)$, $\mathbf{E}_1 = (E, 0)$, $\mathbf{E}_2 = (0, E)$; $E = \Phi + \frac{1}{2}\left(u_1 u^1 + u_2 u^2\right)$ is the energy term. Φ is the geopotential, ζ is the relative vorticity, and f is the Coriolis term.

Vertical Lagrangian Coordinates *(Starr, 1945)*

A "vanishing trick" for vertical advection terms!

- Terrain-following Eulerian surfaces are treated as material surfaces.
- The resulting Lagrangian surfaces are free to move up or down direction.

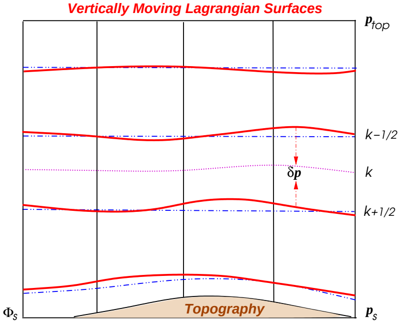

3D Prognostic Equations with Vertical Lagrangian Coordinates

- Lagrangian treatment of the Vertical coordinates results in $\dot{\eta} = 0$ and the mass function $m = \sqrt{G}\delta p = \Delta p$ (pressure thickness).
- Contravariant formulation preserves the familiar "vector invariant" form for the momentum equations.

Momentum Equations: No explicit vertical advection terms

$$\begin{aligned}
\frac{\partial u_1}{\partial t} + \nabla_c \cdot \mathbf{E}_1 &= \sqrt{G}u^2\,(f+\zeta) - R\,T\frac{\partial}{\partial x^1}(\ln p) \\
\frac{\partial u_2}{\partial t} + \nabla_c \cdot \mathbf{E}_2 &= -\sqrt{G}u^1\,(f+\zeta) - R\,T\frac{\partial}{\partial x^2}(\ln p)
\end{aligned}$$

$$\nabla_c \equiv \left(\frac{\partial}{\partial x^1}, \frac{\partial}{\partial x^2}\right), \quad \mathbf{E}_1 = (E, 0),\ \mathbf{E}_2 = (0, E),$$

$$E = \Phi + \frac{1}{2}\left(u_1 u^1 + u_2 u^2\right)$$

3D Prognostic Equations: Flux-Form Continuity Equations

Temperature field is advected with the mass variable Δp

$$\frac{\partial}{\partial t}(\Delta p) + \nabla_c \cdot \left(\mathbf{U}^i\, \Delta p\right) = 0$$
$$\frac{\partial}{\partial t}(\Theta \Delta p) + \nabla_c \cdot \left(\mathbf{U}^i\, \Theta\, \Delta p\right) = 0$$
$$\frac{\partial}{\partial t}(q\, \Delta p) + \nabla_c \cdot \left(\mathbf{U}^i\, q\, \Delta p\right) = 0$$

where $\mathbf{U}^i = \left(u^1, u^2\right)$, $\Delta p = \sqrt{G}\delta p$, δp is the pressure thickness, and Θ is the potential temperature.

Vertical layers are coupled with the hydrostatic relations:

$$\Delta \Phi = -C_p \Theta \Delta \Pi, \quad \Delta \Phi = -RT\Delta \ln p$$

where $\Pi = (p/p_0)^\kappa$ and T Denotes the layer mean temperature.

The Remapping of Lagrangian Variables

Vertically moving Lagrangian Surfaces

- Over time, Lagrangian surfaces deform and thus must be remapped.
- The velocity fields (u_1, u_2), and total energy (Γ_E) are remapped onto the reference coordinates using the 1-D conservative cell-integrated semi-Lagrangian (CISL) method (*Nair & Machenhauer, 2002*)

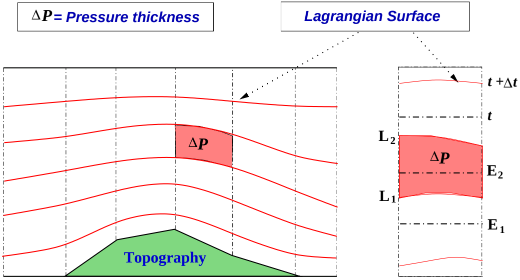

Terrain–following Lagrangian control–volume coordinates

Computational Grid Structure for DG-3D Model

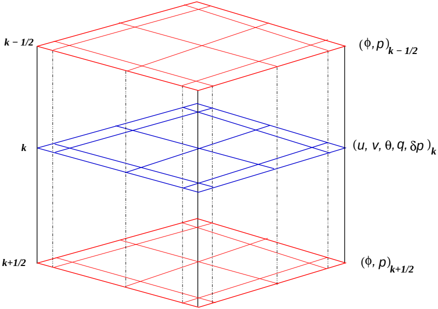

GLL− Grid box

- The prognostic variables u_1, u_2, δp, Θ and q are staggered w.r.t p and ϕ.
- The remapping frequency is $\mathcal{O}(10) \times \Delta t$
- Potential temperature Θ is retrieved from the remapped total energy $\Gamma_E = c_p T + \frac{\delta(p\phi)}{\delta p} + K_E$

The Vertical Lagrangian Dynamics

The hydrostatic pressure at Lagrangian surface, *Lin (MWR, 2004)*

$$p_\ell = p_{top} + \sum_{k=1}^{\ell} \delta p_k, \quad \ell = 1, 2, 3, ..., N$$

where p_{top} represents the pressure at the model top, p_ℓ denotes the pressure at each Lagrangian surface. There are total $N+1$ Lagrangian surfaces span N layers.

The geopotential height at Lagrangian surface:

$$\Phi_\ell = \Phi_s + \sum_{k=N}^{\ell} \Delta\Phi_k, \quad \ell = N, N-1, ..., 1$$

where Φ_s represents the surface geopotential height at the model bottom and Φ_ℓ denotes the geopotential height at each Lagrangian surface.

DG-3D Model Horizontal Aspects: Shallow Water Model

Flux-form SW equations (Vector invariant form)

Nair et al. (MWR, 2005)

$$\begin{aligned}
\frac{\partial u_1}{\partial t} + \frac{\partial}{\partial x^1} E &= \sqrt{G}\, u^2 (f + \zeta) \\
\frac{\partial u_2}{\partial t} + \frac{\partial}{\partial x^2} E &= -\sqrt{G}\, u^1 (f + \zeta) \\
\frac{\partial}{\partial t}(\sqrt{G}\, h) + \frac{\partial}{\partial x^1}(\sqrt{G}\, u^1 h) + \frac{\partial}{\partial x^2}(\sqrt{G}\, u^2 h) &= 0
\end{aligned}$$

where $G = \det(G_{ij})$, h is the height, f Coriolis term; energy term and vorticity are defined as

$$E = \Phi + \frac{1}{2}\left(u_1\, u^1 + u_2\, u^2\right),\ \zeta = \frac{1}{\sqrt{G}} \left[\frac{\partial u_2}{\partial x^1} - \frac{\partial u_1}{\partial x^2}\right].$$

DG-3D Model: Computational Domain

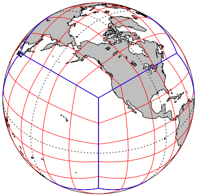

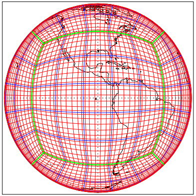

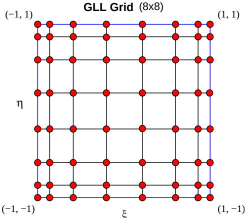

Cubed-Sphere ($N_e = 5$) with 8×8 GLL points

Flux is the only "communicator" at the element edges

- Each face of the cubed-sphere is partitioned into $N_e \times N_e$ rectangular non-overlapping elements (i.e., total $6 \times N_e^2$).
- Each element is mapped onto the Gauss-Lobatto-Legendre (GLL) grid defined by $-1 \leq \xi, \eta \leq 1$, for integration.

Horizontal Advection: Moving Vortices on the Sphere

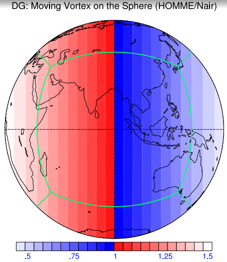

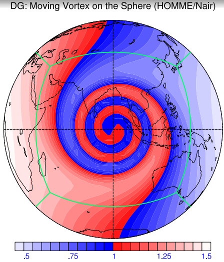

Initial field and DG solution after 12 days. Max error is $\mathcal{O}(10^{-5})$

Deformational Flow Test: *Nair & Jablonowski (MWR, 2007)*

- The vortices are located at diametrically opposite sides of the sphere, the vortices deform as they move along a prescribed trajectory.
- Analytical solution is known and the trajectory is chosen to be a great circle along the NE direction ($\alpha = \pi/4$).

SW Test-2: Geostrophic Flow *(Nair et al., MWR 2005)*

- High-order accuracy and spectral convergence

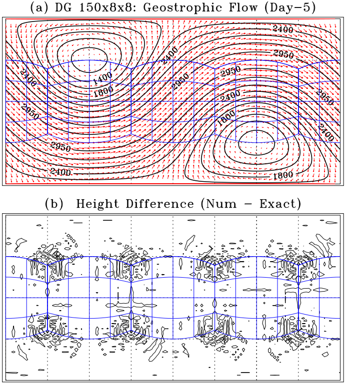

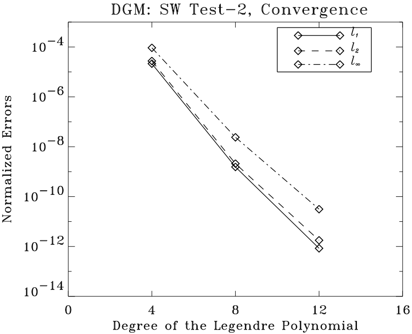

Steady state geostrophic flow ($\alpha = \pi/4$). Max height error is $\mathcal{O}(10^{-6})$ m.

SW Test-5: Flow over a Mountain *(Dennis et al. 2006)*

- No "spectral ringing" for the height fields

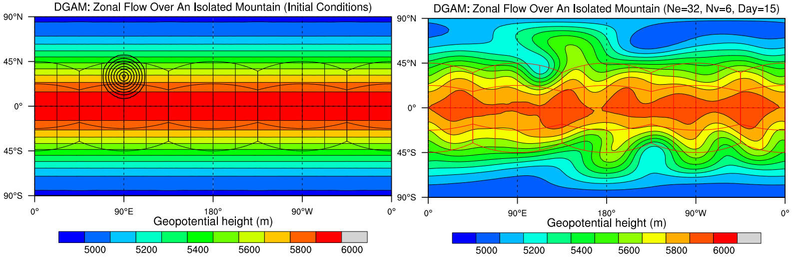

Flow over a mountain ($\approx 0.5^o$). Initial height field (left) initial and after 15 days of integration (right)

DG-3D: Baroclinic Instability Test

(JW-Test) Jablonowski & Williamson *(QJRMS, 2006)*

- To assess the evolution of an idealized baroclinic wave in the Northern Hemisphere.
- The initial conditions are quasi-realistic and defined by analytic expressions. Analytic solutions do not exist.

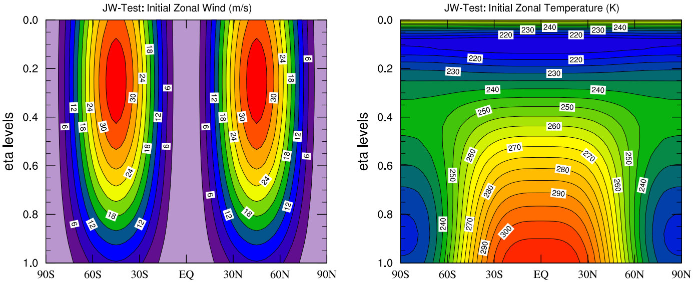

Initial Conditions

JW-Test: Evolution of Surface Pressure over the NH

- Baroclinic waves are triggered by perturbing the velocity field at (20°E, 40°N)
- This test case recommends up to 30 days of model simulation
- Ne = Nv = 8 (approx. 1.6°) with 26 vertical levels and $\Delta t = 30$ Sec.

DG [Ne=8,Nv=8,Nl=26], Ps(hPa) 1H

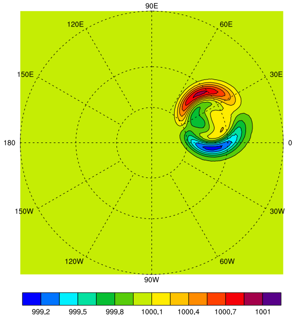

DG [Ne=8,Nv=8,Nl=26], Ps(hPa) 24H

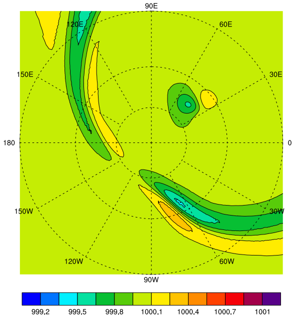

HOMME/DG: Ps(hPa) Day 6 (NH)

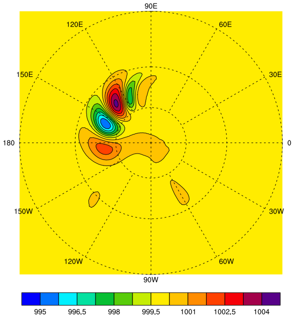

DG-3D Model Vs. NCAR Spectral Model

- The HOMME-DG dynamical core successfully simulates baroclinic instability.

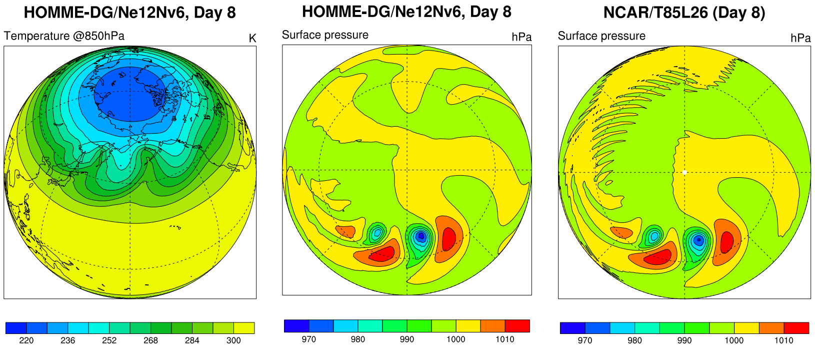

Simulated temperature (K) and surface pressure (hPa) at day 8 for a baroclinic instability test with the HOMME-DG model and the NCAR global spectral model (right). The horizontal resolution is approximately 1.4°.

Note that the DG solution is free of "spectral ringing".

Jablonowski-Williamson Baroclinic Test (Convergence)

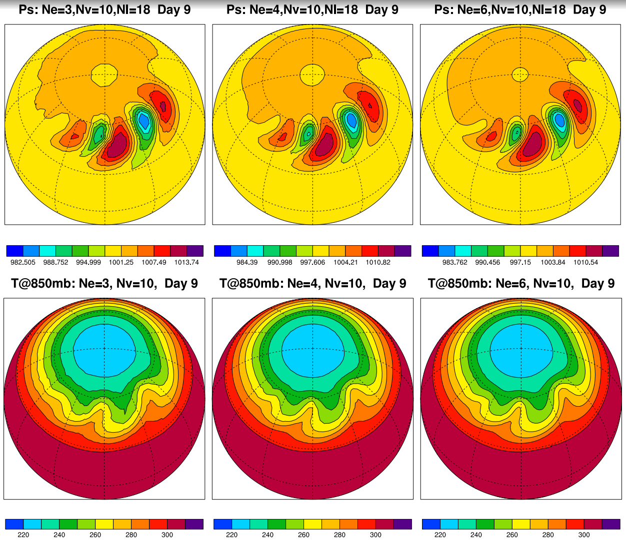

DG Model Vs. NCAR Climate Models (*Nair & Tufo, 2007*)

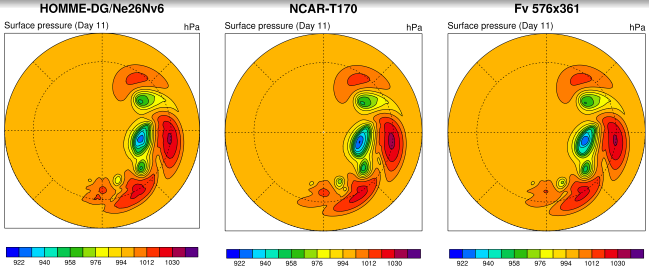

Simulated surface pressure at day 11 for a baroclinic instability test with DG model, and NCAR global spectral model and a FV model. The models use 26 vertical levels and with approximate horizontal resolution of 0.7°.

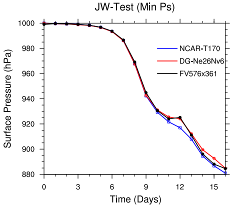

Parallel Performance (3D) - Frost [IBM BG/L]

- DG-3D parallel performance: Sustained Mflops on IBM BG/L (1024 DP nodes, 700 MHz PPC 440s): Approx. 9% peak
- Held-Suarez (preliminary) test: 800 days idealized climate simulation (1° resolution, 26 vertical levels, $\Delta t = 10$ Sec)

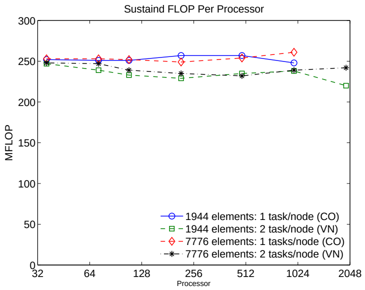

Parallel performance (strong scaling) results for JW-Test

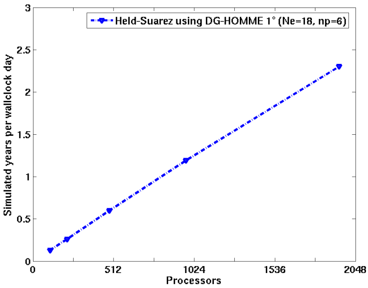

Held-Suarez test (800 days) .

Summary

- The DG-3D model successfully simulates the Baroclinic instability test and the results are comparable with that of the NCAR global spectral model.
- The preliminary scaling results are impressive and comparable to the SE version in HOMME.
- The explicit R-K time integration scheme is robust for the DG-3D model, but very time-step restrictive.
- More efficient time integration schemes are required for practical climate simulations. Possible approaches: Semi-implicit, IMEX-RK, Rosenbrock with optimized Schwarz, etc..
- Future Work: Coupling of the CAM/CCSM *physics* for the *real* climate simulations in HOMME. Targeting for large-scale parallelism with $\mathcal{O}(100K)$ processors.